CrystEngComm

Accepted Manuscript

ROYAL SOCIETY OF CHEMISTRY

www.rsc.org/crystengcomm

Journal Name

ARTICLE

Design Mass-controllable $NiCo_2S_4$/Ketjen Black Nanocomposite Electrodes for High performance Supercapacitors

Received 00th January 20xx,
Accepted 00th January 20xx

DOI: 10.1039/x0xx00000x

www.rsc.org/

Tao Peng,[a] Tieliang Zhao,[b] Qing Zhou,[c] Hongyan Zhou,[c] Jun Wang,*[a] Jinyuan Liu,[a] Qi Liu[a]

$NiCo_2S_4$/Ketjen Black nanocomposites have been successfully fabricated on nikcel foams by a facile two-step solution-based method. Compared with the pure $NiCo_2S_4$ electrode (Ni_1K_0), the $NiCo_2S_4$/KB nanocomposite electrodes ($Ni_1K_{0.5}$, $Ni_1K_{0.25}$, $Ni_1K_{0.125}$) with controllable mass loadings show significantly enhanced electrochemical performance. Electrochemical measurements demonstrate that the $Ni_1K_{0.25}$ electrode has a competitive areal specific capacitance (10.10 F cm^{-2} at 10 mA cm^{-2}), good rate capacitance (38.41% capacitance retention at 40 mA cm^{-2}) and excellent cycling stability (92.1% capacitance retention 6000 cycles at 10 mA cm^{-2}). Such high performance may promote the $NiCo_2S_4$/KB nanocomposite in practical application for supercapacitors.

1. Introduction

In recent years, high-performance energy storage devices are urgently needed due to the ubiquity of mobile devices and the growing concerns on the depletion of fossil fuels.[1-3] Pseudocapacitors, also called electrochemical capacitors, are attracting special attention with reasonably high power, high energy densities and life span.[4-12] Therefore, they have potential to bridging the gap between conventional capacitors and batteries.

As a kind of pseudocapacitive material, nickel cobalt sulfide ($NiCo_2S_4$) has been widely explored for its high conductivity and rich redox ability.[13-25] Recently, significant progress has been achieved in enhancing the specific capacitance of $NiCo_2S_4$-based electrodes.[16-20] Extensive efforts have been focused on controlling the architecture of $NiCo_2S_4$-based materials to balance ionic and electron transporting.[13-15] In fact, $NiCo_2S_4$-based materials have achieved greatly success with respect to robust interfaces and excellent performance via two powerful strategies.[13-25] One way is that directly growth of nanostructured materials on substrates. For example, Xiao et al. have synthesized $NiCo_2S_4$ nanotube arrays on carbon fiber paper and obtained a high areal capacitance of 2.86 F cm^{-2} at 4 mA cm^{-2}.[15] More recently, Alshareef and his co-workers have fabricated $NiCo_2S_4$ nanosheet arrays electrode with specific capacitance of 1418 F g^{-1} at 5 A g^{-1} via an electrodeposition method.[17] Although the as-obtained additive-free electrodes show enhanced power density due to low resistance, relatively low mass loadings may limit their practical applications. What's more, the hydrothermal method generally requires high temperature, high pressure and long reaction time.[17-20] Therefore, it is pressing to search for a facile and environmental-friendly method which can simultaneously guarantee high mass of nanostructured $NiCo_2S_4$ loading on substrates and high conductivity of the as-obtained electrodes.

Another way is that assembling scrupulous designed $NiCo_2S_4$-based nanoarchitectures on substrates via slurry-pasting. Slurry casting method could achieve high specific capacitance at the cost of bulk agglomeration and extra weight of additives.[13-15] However, the lack in spatial precision may eradicate the advantages of nanostructured materials. As a result, a key challenge in the fabrication of electrodes lies in stepwisely constructing optimal physical space with a large mass loading.

As a proof-of-concept, we present a two-step method to produce $NiCo_2S_4$/Ketjen Black nanocomposite electrodes with controllable mass loadings (Sch.1). Firstly, the 3D interconnected flower-like Ni-Co precursors have been directly grown on the nickel foam via a facile modified solution-based method. The substrate which was closely covered with the as-obtained Ni-Co precursors could provide robust interfaces. Secondly, considering that high mass loadings always lead to poor ion and electron transporting, conductive Ketjen Black (KB) has been added to $NiCl_2/CoCl_2$ solution and the Ni-Co precursor/KB composite has been synthesized by the following coprecipitation method. Through a dip–dry process and anion exchange reaction (AER), $NiCo_2S_4$/KB composite was successfully assembled on the nickel foams. High mass loadings of the electrode could be achieved with increased

[a] Key Laboratory of Superlight Material and Surface Technology, Ministry of Education, Harbin Engineering University, 150001, PR China. E-mail: zhqw1888@souhu.com.Tel.: +86 451 8253 3026; Fax: +86 451 8253 3026;
[b] College of Mechanical and Electrical Engineering, Harbin Engineering University, 150001, PR China.
[c] Southwest University of Science and Technology, Mianyang, 621010,P.R.China
Electronic Supplementary Information (ESI) available.See DOI: 10.1039/x0xx00000x

dipping numbers. As a result, the unique electrode ($Ni_1K_{0.25}$) has shown high areal specific capacitance (10.10 F cm^{-2} at 10

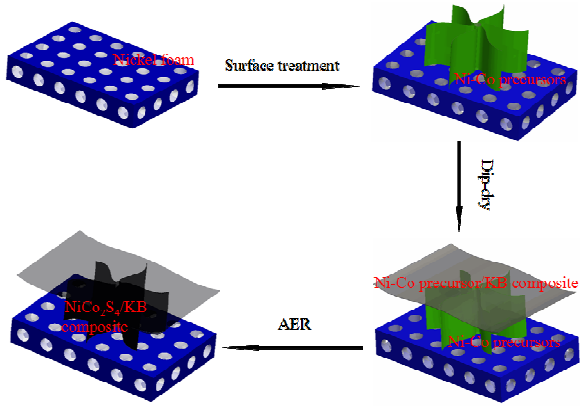

Sch.1 Schematic image of fabricating mass-controllable $NiCo_2S_4$/Ketjen Black nanocomposite electrodes.

mA cm^{-2}), good rate capacitance (38.41% capacitance retention at 40 mA cm^{-2}) and excellent cycling stability (92.1% capacitance retention 6000 cycles at 10 mA cm^{-2}), which may promote it a promising electrode for supercapacitors.

2. Experimental

All the chemicals were directly used after purchase without any further purification.

2.1 Surface modification of KB

Ketjen Black (KB) is a kind of carbon black with high conductivity. Surface modification was performed to address the hydrophobic problem of KB.[26] 10 g KB was dispersed into 1 L HNO_3 (20 wt %) to form a homogeneous black solution. Then, the black solution was heated to 80 □ under continuous stirring. After reaction for 3 h, the resultant product was obtained by centrifugation/washing/redispersion with deionized water until the filtrate was neutral. This modified KB was noted as m-KB.

2.2 Surface treatment of nickel foam

Surface treatment of nickel foam was performed via a method which was reported in the literature with minor modifications.[27] Nickel foams (50 × 25 × 1 mm^3, pores per inch: 110) were rolled to a thickness of 0.5 mm before use. The rolled nickel foams were immersed in a 3 M HCl solution for 15 min, and then soaked in a 0.02 M $NiCl_2$ solution to prevent oxidation. 1 mmol $Ni(NO_3)_2 \cdot 6H_2O$ and 2 mmol $Co(NO_3)_2 \cdot 6H_2O$ were fully dispersed into a mixed solution of 20 mL ethanol and 40 mL deionized water, followed by the addition of 6 mmol hexamethylenetetramine. A piece of nickel foam was dipped into a bottle (80 mL in capacity) which contains the above solution. Then, the bottle was capped and heated to 90□ in a water bath for 2.5 h. The nickel foam substrate with Ni-Co precursors was removed and washed with deionized water and absolute ethanol, respectively, then dried at 90 □ for further treatment.

2.3 Stepwisely assembly of Ni-Co precursor/KB composite on nickel foam

In a typical procedure, 26.68 mmol $NiCl_2 \cdot 6H_2O$ and 53.32 mmol $CoCl_2 \cdot 6H_2O$ were dispersed in 200 mL deionized water to form a clear pink solution. The pink solution was then transferred to four beakers (150 mL in capacity) with the same volume (50 mL). Subsequently, 3.71 mL, 1.82 mL, 0.92 mL and 0 mL m-KB solution (10.8 mg mL^{-1}) were added to the above beakers, respectively. After that, 1.9 g of NaOH in 50 mL ethanol was dropwisely added to the above beakers with vigorous stirring. The mixtures were digested for 0.5 h under continuous stirring until the suspensions were formed.

Stepwisely assembly of Ni-Co precursor/KB on nickel foam was performed by a dip-dry method which was reported in our previous work.[28] The treated nickel foams were dipped into the above suspensions, then immediately removed. After drying at 90 □ for 15 min, the same process could be repeated to increase the mass loading of nickel foams. The nickel foams with loaded Ni-Co precursor/KB composite were rinsed with deionized water and ethanol to remove residual ions.

2.4 Preparation of $NiCo_2S_4$/KB composite electrode

The as-prepared Ni-Co precursor/KB composite electrodes were dipped into a beaker with 0.05 M (150 mL) of Na_2S solution. Then, the beaker was heated to 90 ℃ in a water bath for 9 h. After the AER process, the nickel foams with loaded products were removed and rinsed with deionized water and absolute ethanol, respectively, then dried at 90 ℃.

The as-prepared $NiCo_2S_4$/KB composite electrodes which were obtained by dipping from the Ni-Co precursor/KB suspensions with different mole fraction were noted as $Ni_1K_{0.5}$, $Ni_1K_{0.25}$, $Ni_1K_{0.125}$, Ni_1K_0.

2.5 Characterization

The crystal structure and phase of the as-prepared materials were investigated by X-ray diffraction (XRD) (Rigaku TTR-III, Cu K_α, λ = 0.15406 nm) with 2θ ranging from 10° to 80°. The morphology of the as-obtained samples were characterized by scanning electron microscopy-energy dispersive spectroscopy equipped with an energy-dispersive X-ray spectrometer (SEM-EDS) (JEOL JSM-6480A) and trans-mission electron microscopy (TEM) (Philips CM 200 FEG, 200 kV). The N_2 sorption measurements were conducted using TriStar II 3020 2.00 instrument at 195.850 °C (77 K). The near-surface elemental composition of the $NiCo_2S_4$ product was measured by X-ray photoelectron spectroscopy (XPS) (PHI 5700 ESCA System). The $NiCo_2S_4$/KB composite $Ni_1K_{0.125}$ has been applied to the XRD, XPS, EDS, TEM and N_2 sorption measurement.

2.6 Electrochemical measurements

A three-electrode system which consisted of a working electrode, a platinum foil counter electrode (1 × 1 cm^2), a

saturated calomel electrode (SCE) reference electrode, and electrolyte (6 M KOH aqueous solution) was used in the measurements. The as-prepared electrodes with nominal area of 1×1 cm^2 were served as working electrode. The mass loadings of the $NiCo_2S_4$/KB composite electrodes were 6.512, 6.472, 6.512 mg cm^{-2} for $Ni_1K_{0.5}$, $Ni_1K_{0.25}$, $Ni_1K_{0.125}$, respectively. To compare with $Ni_1K_{0.5}$, $Ni_1K_{0.25}$, $Ni_1K_{0.125}$, the corresponding $NiCo_2S_4$ electrode (Ni_1K_0) with mass loading of 6.520 mg cm^{-2} also measured under the same condition. Cyclic voltammetry (CV) and galvanostatic charge-discharge (GCD) were performed on a CHI 660D electrochemistry workstation. Electrochemical impedance spectroscopy (EIS) measurements were conducted in the frequency range of 0.005 Hz to 100 kHz at the open circuit potential.

2.7 Calculations

For galvanostatic charge-discharge curves, the areal specific capacitance C_s (F cm^{-2}), the gravimetric specific capacitance C_m (F g^{-1}), equivalent series resistance R_{ESR} (Ω) and columbic efficiency (η) can be evaluated by the following equations (1)-(4), respectively:

$$C_S = \frac{It}{A\Delta V} \quad (1)$$

$$C_{\mathrm{m}} = \frac{It}{m\Delta V} \quad (2)$$

$$R = \frac{V_{\mathrm{drop}}}{2I} \quad (3)$$

$$\eta = \frac{\mathrm{t}_C}{t}\times 100\% \quad (4)$$

where I (A) is the discharge current, t is the discharge time (s), ΔV is the applied potential region (V), A refers to the area (cm^2) of the electrode, m (g) is the mass of the active materials, and V_{drop} (V) is estimated from the voltage drop at the beginning of the discharge curve, η (%) is columbic efficiency, t_c is the charge time (s).

3. Results and discussion

3.1 Synthesis of $NiCo_2S_4$/KB nanocomposites and their characterization

As a cost-effective conductive material, KB was widely applied in the field of lithium ion batteries[29], electrocatalysis[30] and supercapacitors[31] due to its large specific surface area (about 1270 m^2 g^{-1}) and high conductivity. However, its hydrophobic property greatly hinders the hybrid process in our work.[26] Therefore, surface modification treatment was performed by introduce the carboxylic moiety (-COOH) to KB. As shown in Fig.S1, the FT-IR spectrum of KB and m-KB confirm the surface modification process. From the FT-IR spectrum of m-KB, the new bonds at 3423 cm^{-1} and 1720 cm^{-1} could be attribute to the stretching vibrations of the -OH and C=O, respectively. It indicates that the existence of the carboxylic moiety (-COOH) in m-KB, which did not appeared in the original KB.[26] Therefore, the surface modification treatment of KB could highly facilitate hybrid m-KB to Ni-Co precursors.

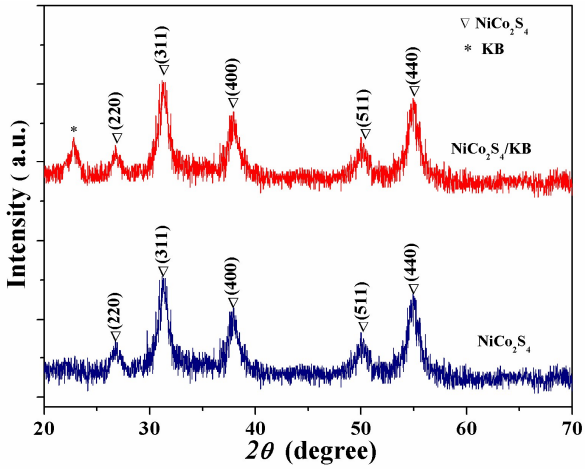

Fig.1 XRD patterns of the $NiCo_2S_4$/KB nanocomposite (in red) and the corresponding $NiCo_2S_4$ (in blue).

After adding m-KB to $NiCl_2/CoCl_2$ solution, Ni-Co precursor/KB composite was obtained in the following coprecipitation process. By AER, Ni-Co precursor/KB composites could be easily converted to the corresponding $NiCo_2S_4$/KB composites. XRD patterns of the $NiCo_2S_4$/KB nanocomposite (in red) and the corresponding $NiCo_2S_4$ (in blue) could confirm the formation of $NiCo_2S_4$/KB composite. The peaks located at 2θ values of 26.8°, 31.5°, 38.5°, 50.4° and 55.2° correspond to the (220), (311), (400), (511) and (440) diffraction planes of the cubic phase $NiCo_2S_4$ (JCPDF 43-1477) [25]. According to the previous reports,[26, 31] the only characteristic peak of which was marked with "*" can be well indexed to KB. Based on the above analysis, relative high purity $NiCo_2S_4$/KB nanocomposite was obtained via our proposed synthesis method.

The X-ray photoelectron spectroscopy (XPS) measurementwas carried out to futher understand the composition of the $NiCo_2S_4$/KB nanocomposite sample (Fig.2). The survey spectrum (Fig.S2) indicates the presence of Ni, Co, S and C element. The Ni 2p spectrum was well fitted with two spin-orbit doublets, which are characteristic of two shake-up satellites $Ni^{2+}$and Ni^{3+}.[14] Simultaneously, the Co 2p spectrum also shows two spin-orbit doublets, which contains a high energy band (Co $2p_{1/2}$) and a low energy band (Co $2p_{3/2}$) at 798.5 eV and 783.6 eV, respectively. The spin-orbit splitting values of Co $2p_{1/2}$ and Co $2p_{3/2}$ are over 15 eV, confirming the presence of Co^{2+} and Co^{3+}.[25] As for S 2p spectrum, the peak at 161.8 eV is characteristic of S^{2-} while the component at 162.9

eV can be attributed to the sulphion in low coordination.[15] Moreover, three peaks of the C 1s spectrum at 284.9, 286.8 and 288.5 eV also could assigned to the carbon atoms of the Ketjen black, those of ether carbons and those of carboxyl carbons.[6]

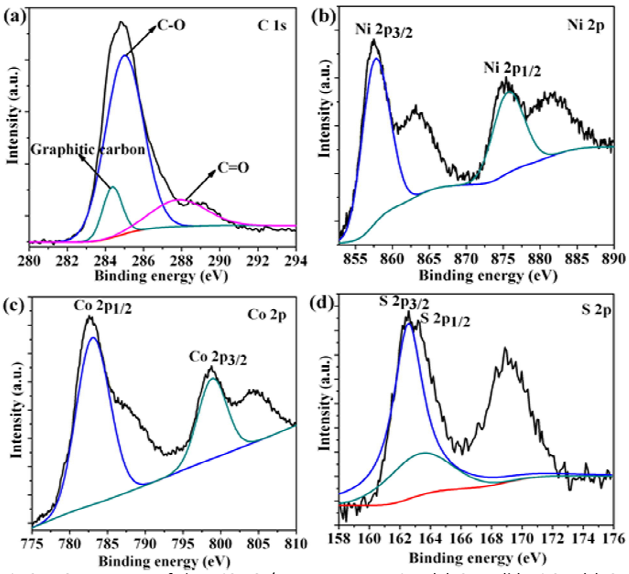

Fig.2 XPS spectrum of the $NiCo_2S_4$/KB nanocomposite :(a) C 1s; (b) Ni 2p; (c) Co 2p; (d) S 2p.

According to the above XPS analysis, the $NiCo_2S_4$/KB nanocomphosite sample has a composition of Co^{2+}, Co^{3+}, Ni^{2+}, Ni^{3+}, S^{2-} and C, which is consistent with the XRD analysis.

In the first step, 3D interconnected flower-like $NiCo_2S_4$ nanosheets have been directly grown on nickel foams via a facile modified solution-based method and subsequently anion exchange reaction (AER). SEM images of the $NiCo_2S_4$ nanosheets on nickel foams (Fig.3a-b) could fully confirm the surface treatment process of nickel foam. The $NiCo_2S_4$ nanosheets are uniformly covered with the skeleton of nickel foams (Fig.3a). When the SEM image of Fig.3a was magnified (a1), 3D interconnected flower-like $NiCo_2S_4$ nanosheets can be observed. Although the above step provides robust contact between active materials and substrate which could highly facilitate the following step, relatively low mass loadings were achieved. Therefore, the second step was performed to enhance mass loadings of nickel foam. In the second step, $NiCo_2S_4$/KB nanocomposites with different mole fraction were successfully assembled on the above nickel foams. From Fig.3c-d, it can be observed that a little quantity of the pure $NiCo_2S_4$ (Ni_1K_0) synthesized by the coprecipitation and AER method was loaded on the surface treated nickel foams and the 3D interconnected flower-like $NiCo_2S_4$ nanosheets merely grow densely. However, a large quantity of $NiCo_2S_4$/KB composites was covered on the substrate (Fig.3e-h). The stepwise self-assembled nanosheets became more compact and filled the pores of the above 3D interconnected flower-like $NiCo_2S_4$ nanosheets, leading to the increase of mass loading. The energy-dispersive X-ray spectrometer (EDS) measurement was conducted in the section of g1 (Fig.3g) to futher confirm the composition of the as-prepared sample. Only the peaks of C, Ni, Co, S elements appear in the EDS patterns (Fig.S3), revealing that the as-prepared sample mainly contains C, Ni, Co, S elements. The elemental ratio of Ni, Co, S is about 1: 2.03: 4.07, matching well with the formula of $NiCo_2S_4$. Obviously, the as-prepared sample is almost constituted by $NiCo_2S_4$ and KB. [25]As a result, the $NiCo_2S_4$/KB nanocomposite electrodes with high loadings were fabricated by the two-step method.

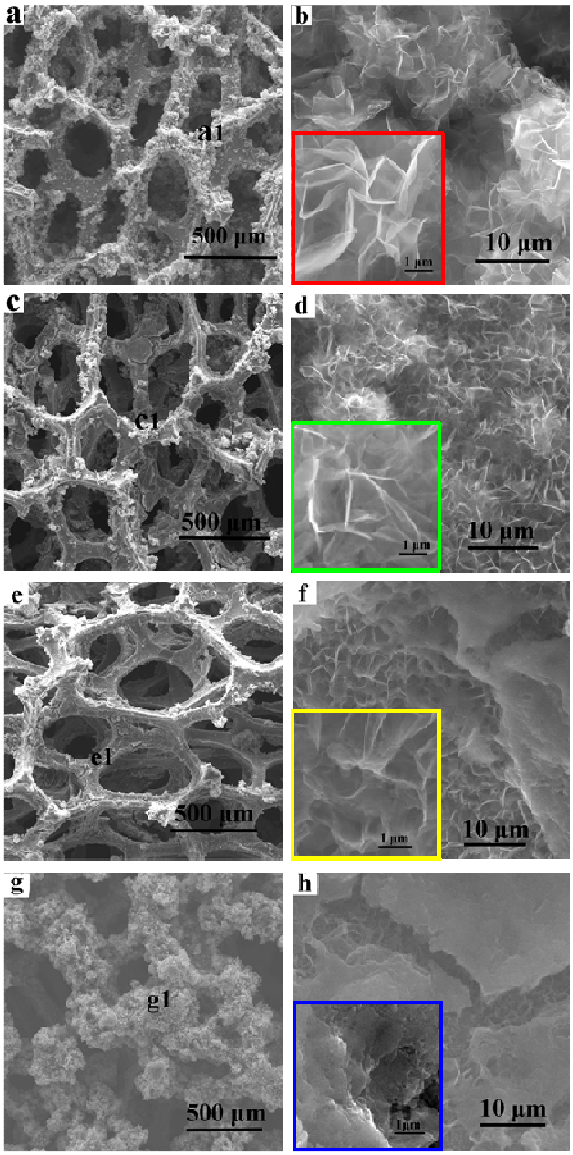

Fig.3 (a)(b) SEM image of flower-like $NiCo_2S_4$ nanosheets on nickel foams; (c)(d) SEM image of $NiCo_2S_4$ loaded on the surface-treated nickel foams (Ni_1K_0) (Dipping number: 1); (e)(f) SEM image of $NiCo_2S_4$/KB nanocomposites loaded on the surface-treated nickel foams ($Ni_1K_{0.25}$) (Dipping number: 1); (g)(h) SEM image of $NiCo_2S_4$/KB nanocomposites loaded on the surface-treated nickel foams (Dipping number: 4)

The TEM images were applied to further analyze the microstructure of the as-obtained $NiCo_2S_4$/KB nanocomposite samples. From Fig.4a-c, it can be seen that the m-KB

microspheres were contacted with the $NiCo_2S_4$ nanosheets. As reported in previous works, the carboxylic moiety (-COOH) on the KB surface may combine with $NiCo_2S_4$ to form chemical bonds, ensuring more tight contacts between $NiCo_2S_4$ and KB.[31] When the TEM images of Fig.4c were magnified, it was clearly observed that the lattice fringes were appeared in the $NiCo_2S_4$ nanosheet, showing its high crystallinity (Fig.4d). The special structure of $NiCo_2S_4$/KB nanocomposite may provide shortened pathways and facilitates effective electrolyte penetration, consequently leading to improved capacitance and cycling stability.[15-20]

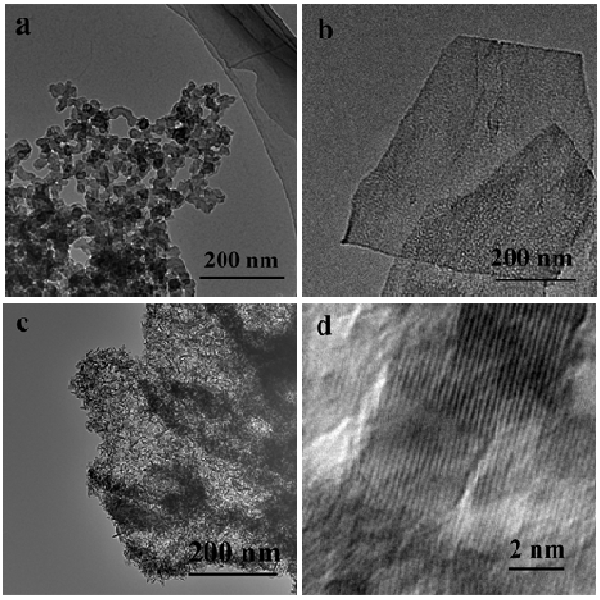

Fig. 4 (a) TEM image of m-KB; (b) TEM images of $NiCo_2S_4$ nanosheets; (c)(d) TEM images of $NiCo_2S_4$/KB nanocomposites

The N_2 sorption measurement was conducted to evaluate the Brunauer-Emmett-Teller (BET) surface area and pore-size distribution of the as-prepared $NiCo_2S_4$/KB nanocomposite samples. Comparing to the pristine $NiCo_2S_4$ (35.20 m^2/g), the surface areas of $NiCo_2S_4$/KB nanocomposite (104.37 m^2/g) was highly enhanced due to the introduction of m-KB (Fig.S4a). The $NiCo_2S_4$/KB nanocomposite sample with a pore size range of 4-5 nm can be confirmed by the pore-size distribution analysis (Fig.S4b).

3.2 Control of mass loading on nickel foam via a dip–dry process

The mass loadings of $NiCo_2S_4$/KB nanocomposite on nickel foam could be well-controlled by a dip–dry process which was reported in our previous work. As depicted in Fig.3e-g, the $NiCo_2S_4$/KB nanocomposites were gradually covered on the skeleton of nickel foams and filled the free pore volume of the nickel foams with the dipping number increased. The mass loading of the as-prepared electrodes were uniformly increased during each dip-dry process, showing its high controllability (Fig.5). Low mass volatility in the process also reveals that the experimental results could be easily repeated, which is very important for scale-up.[25,31]

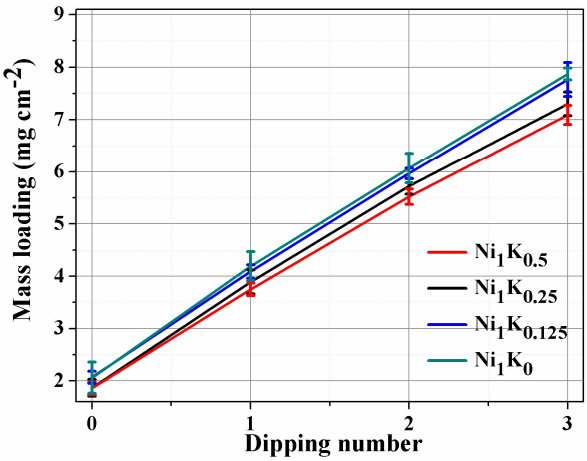

Fig.5 Mass loadings of $NiCo_2S_4$/KB nanocomposite on nickel foams.

3.3 Electrochemical performance of the as-prepared electrodes

The $NiCo_2S_4$/KB nanocomposites loaded on nickel foam were directly used as working electrode in a three-electrode system and their electrochemical performance were tested by cyclic voltammetry (CV) and galvanostatic charge/discharge measurements (GCD). Fig.6a shows the cyclic voltammetry (CV) curves at a scan rate of 5 mV s^{-1} in a potential window of 0 to 0.6 V. Clearly, the shapes of the CV curves in Fig.6a are different from the ideal rectangular shapes, revealing the pseudocapacitive characteristics of the $NiCo_2S_4$/KB nanocomposites.[13] A pair of redox peaks (an anodic peak and a cathodic peak) at 0.26 and 0.42 V can be attributed to the following redox reactions of $NiCo_2S_4$: [16-19]

$$CoS + OH^- \leftrightarrow CoSOH + e^-$$

$$CoSOH + OH^- \leftrightarrow CoSO + H_2O + e^-$$

$$NiS + OH^- \leftrightarrow NiSOH + e^-$$

The as-observed redox peaks might be assigned to the redox reaction from $NiCo_2S_4$ to CoSOH and NiSOH due to two redox peaks of $Co^{2+}/Co^{3+}$and Ni^{2+}/Ni^{3+} overlap together.[21] Another pair of redox peaks cannot be observed in the scan rate of 5 mV s^{-1}. As the scan rates increased from 5 to 30 mV s^{-1}, the redox peaks shift to more positive and negative potential, respectively, indicating the reversibility of redox reaction decreased (Fig.S5). It may be caused by OH^- diffusion in the electrodes.[36] The $NiCo_2S_4$ active material could fully react with OH^- ions during the low scan rates. Moreover, in comparison with the single $NiCo_2S_4$ electrode (Ni_1K_0), the integrated CV areas for the $NiCo_2S_4$/KB electrodes ($Ni_1K_{0.5}$, $Ni_1K_{0.25}$, $Ni_1K_{0.125}$) are

relatively larger (Fig.6a). This confirms that the conductive KB could highly enhance the electrochemical performance of $NiCo_2S_4$.[15] It also can be observed that the $Ni_1K_{0.25}$ electrode

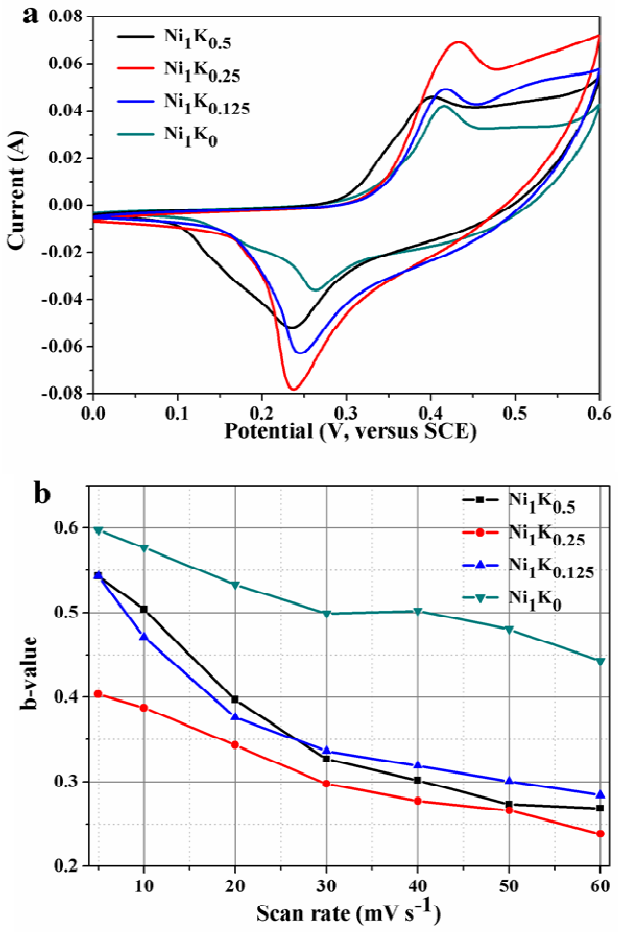

Fig.6 (a) CV spectra of $Ni_1K_{0.5}$, $Ni_1K_{0.25}$, $Ni_1K_{0.125}$ and Ni_1K_0 at 5 mV s^{-1}; (b) b values of $Ni_1K_{0.5}$, $Ni_1K_{0.25}$, $Ni_1K_{0.125}$ and Ni_1K_0 at scan rates between 5 and 60 mV s^{-1}.

show larger integrated CV areas than the $Ni_1K_{0.5}$ and $Ni_1K_{0.125}$ electrodes. Therefore, the $Ni_1K_{0.25}$ electrode is more suitable for supercapactitor.

To further understand the charge storage process, the following Equation 5 has been applied to analyze the CV spectra.[25, 31]

$$I = av^b \qquad (5)$$

Where I (A) is the peak current, v (mV s^{-1}) is scan rate, a and b are variable parameters. Using the parameter of b, the charge storage process could be distinguished between surface-controlled process (b=1) and diffusion-controlled process (b=0.5). The b values for the single $NiCo_2S_4$ electrode (Ni_1K_0) range from 0.6 to 0.5 at a scan rate between 5 and 40 mV s^{-1} (Fig.6b), revealing that the charge storage process is mainly surface-controlled. [25, 31] However, as for the $NiCo_2S_4$/KB electrodes ($Ni_1K_{0.5}$, $Ni_1K_{0.25}$, $Ni_1K_{0.125}$), the b values are not more than 0.5 with the scan rate ranges from 10 and 60 mV s^{-1}. The charge storage process for the $NiCo_2S_4$/KB electrodes is dominated by diffusion. [25, 31] According to the above analysis, it can be concluded that the conductive KB could highly facilitate the electron transporting of the as-prepared electrodes.

Galvanostatic charge/discharge measurements were also performed to evaluate the capacitance performances of the as-prepared electrodes. As shown in Fig.7a and Fig.S6, two distinct plateaus in the charge/discharge curve indicate the existence of redox reactions which is consistent with the above CV results.[32, 36] Moreover, the galvanostatic charge/discharge curves are approximately symmetrical at low current densities, revealing excellent high electrochemical reversibility of the as-prepared electrodes.[13,15] Based on the galvanostatic charge/discharge curves, the specific capacitance can be

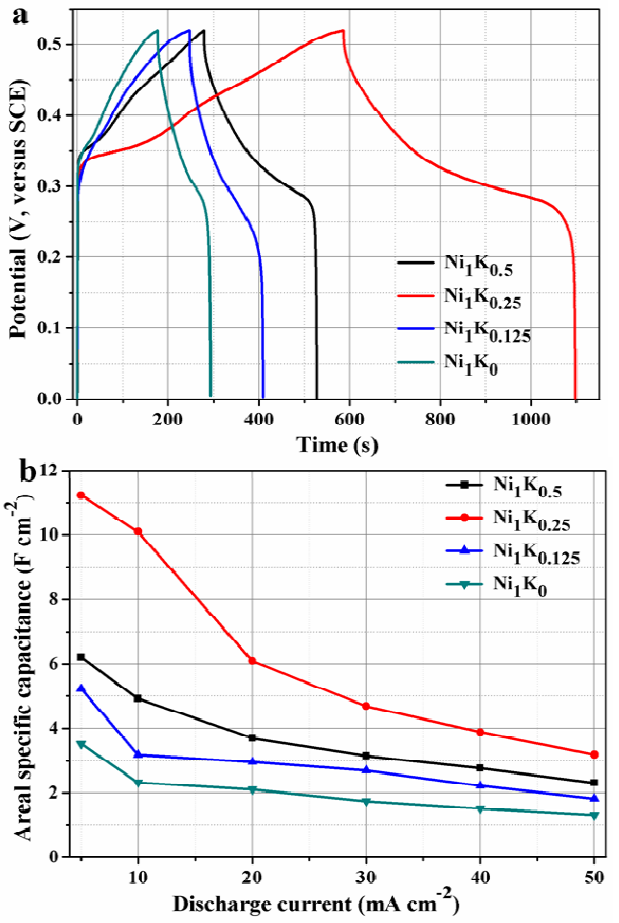

Fig.7 (a) Charge and discharge curves of $Ni_1K_{0.5}$, $Ni_1K_{0.25}$, $Ni_1K_{0.125}$ and Ni_1K_0 at current density of 10 mA cm^{-2}; (b) Areal specific capacitance (C_s) of $Ni_1K_{0.5}$, $Ni_1K_{0.25}$, $Ni_1K_{0.125}$ and Ni_1K_0 at current densities between 5 and 50 mA cm^{-2}, respectively.

calculated by Equation 1 and 2. At the current density of 10 mA cm^{-2}, the areal specific capacitances (C_s) for $Ni_1K_{0.5}$, $Ni_1K_{0.25}$, $Ni_1K_{0.125}$, Ni_1K_0 are about 4.92, 10.10, 3.19, 2.32 F cm^{-2} respectively (Fig.7b) and the corresponding gravimetric specific capacitances (C_m) for $Ni_1K_{0.5}$, $Ni_1K_{0.25}$, $Ni_1K_{0.125}$,

Ni_1K_0 are about 755.77, 1560.27, 489.30, 355.47 F g^{-1} (Fig.S7). Evidently, the $NiCo_2S_4$/KB electrodes deliver higher specific capacitance than the bare $NiCo_2S_4$ electrode. Meanwhile, the areal specific capacitance of the $Ni_1K_{0.25}$ electrode is also larger than the $Ni_1K_{0.5}$ and $Ni_1K_{0.125}$ electrodes. The specific capacitances gradually decrease with an increase in current density, which also can be attributed to the low OH^- diffusion.[13] However, the $Ni_1K_{0.25}$ electrode shows a remarkable areal capacitance of 3.88 F cm^{-2} even when the current density is up to 40 mA cm^{-2}. As a result, the $Ni_1K_{0.25}$ electrode indicates a relative high capacitance retention (38.41%) at 40 mA cm^{-2} , showing its good rate capability. Such high areal specific capacitance of the $Ni_1K_{0.25}$ electrode reported here is competitive to other previous reported $NiCo_2S_4$-based nanoarchitectures (Tab.S1), such as $NiCo_2S_4$ nanotube arrays[15] (2.86 F cm^{-2} at 4 mA cm^{-2}), $NiCo_2S_4$ nanoplates[36] (1.05 F cm^{-2} at 2.4 mA cm^{-2}).

To futher evaluate the electrochemical performance of the as-prepared electrodes, electrochemical impedance spectroscopy (EIS) were carried out at open circuit potential. Fig.8 shows the Nyquist plots of the as-prepared electrodes ($Ni_1K_{0.5}$, $Ni_1K_{0.25}$, $Ni_1K_{0.125}$, Ni_1K_0), which were composed of a quasi-semicircle at high frequency region and a sloped line at low frequency region. The slops of the four straight lines are almost the same, showing that the electrolyte diffusion impendence values for the as-prepared electrodes are nearly equal.[33-35] The x-intercept at the real part (Z') of the Nyquist plot, which is a combined resistance (R_e) from the ionic resistance of the electrolyte, contact resistance at the active material/current collector interface and intrinsic resistance of the active materials, has a significant influence on the capacitive performance of the electrode materials.[35] Here, the values of R_e for $Ni_1K_{0.5}$, $Ni_1K_{0.25}$, $Ni_1K_{0.125}$, Ni_1K_0 are about 0.8, 0.72, 0.78 and 0.83 Ω, respectively. Moreover, the equivalent series resistances of $Ni_1K_{0.5}$, $Ni_1K_{0.25}$, $Ni_1K_{0.125}$, Ni_1K_0 can also be calculated by Equation 3 in the galvanostatic charge/discharge measurements. From Fig.S8, the same conclusion can be obtained that the $NiCo_2S_4$/KB samples are good electrode materials with very small series resistances. Besides, the $NiCo_2S_4$/KB electrodes ($Ni_1K_{0.5}$, $Ni_1K_{0.25}$, $Ni_1K_{0.125}$) have smaller diameters of semicircles, revealing that they have much lower interfacial charge-transfer impedance (R_{ct}) as compared to that of the bare $NiCo_2S_4$ (Ni_1K_0).[35] Therefore, the above analysis clearly demonstrates that the $NiCo_2S_4$/KB electrodes exhibit fast electron transport and favorable charge-transfer kinetics.

The stability of the as-prepared electrodes ($Ni_1K_{0.25}$, Ni_1K_0) was investigated at current density of 10 mA cm^{-2} for 6000 cycles, as shown in Fig.9 and Fig.S9. For the initial 100 cycles, the areal specific capacitance of the as-prepared electrodes slightly increases due to the activation of the $NiCo_2S_4$ material. However, the specific capacitance gradually decreases with the cycle number continue to increasing. Notably, the $Ni_1K_{0.25}$ electrode can still retains 92.1% of the initial specific capacitance after 6000 cycles which is higher than the corresponding Ni_1K_0 electrode (82.7% retention). What's more, the columbic efficiency of the $Ni_1K_{0.25}$ electrode remains higher to 90% during the cycling process. The microstructure of the as-prepared active material is well-retained after 6000 cycles at

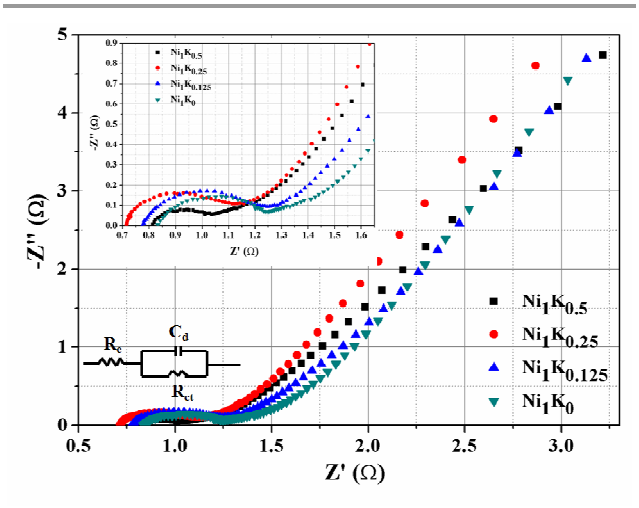

Fig.8 EIS of $Ni_1K_{0.5}$, $Ni_1K_{0.25}$, $Ni_1K_{0.125}$ and Ni_1K_0.

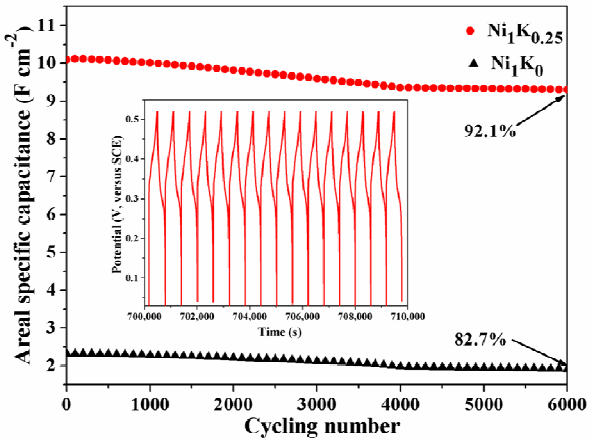

Fig.9 Cycling performance of the as-prepared electrode ($Ni_1K_{0.25}$ and Ni_1K_0) for 6000 cycles at 10 mA cm^{-2}.

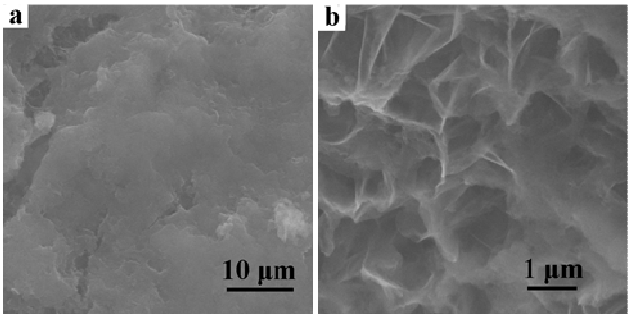

Fig.10 SEM images of the $NiCo_2S_4$/KB nanocomposites on nickel foam after 6000 cycles at 10 mA cm^{-2}.

10 mA cm^{-2} (Fig.10). Such good cycle stability may relate to the stability of the as-obtained microstructure which could guarantee the high reversible redox reaction.[25, 27]

The excellent electrochemical performance of $NiCo_2S_4$/KB nanocomposites can be attributed to the following factors. Firstly, the $NiCo_2S_4$/KB nanocomposites directly grown on nickel foam provides good electrical contacts between active materials and the substrate; [37] Secondly, KB serves as a bridge to provide a more conductive path for electron transporting; [26, 29-31] Thirdly, the microstructures of $NiCo_2S_4$/KB nanocomposites lead to easier electrolyte penetration into the inner region of the electrodes; [13-15, 37] Finally, the enhanced surface area of $NiCo_2S_4$/KB nanocomposites highly favors the redox reactions at or near the surface of the electrodes by providing more electroactive sites. [1, 37]

4. Conclusions

In summary, $NiCo_2S_4$/KB nanocomposites have been successfully fabricated on the surface-treated nikcel foams as a binder-free electrode for high performance supercapacitors. The as-prepared $NiCo_2S_4$/KB nanocomposite electrodes ($Ni_1K_{0.5}$, $Ni_1K_{0.25}$, $Ni_1K_{0.125}$) with controllable mass loadings show significantly enhanced electrochemical performance compared with the pure $NiCo_2S_4$ electrode (Ni_1K_0). Electrochemical measurements demonstrate that the $Ni_1K_{0.25}$ electrode has a competitive areal specific capacitance (10.10 F cm^{-2} at 10 mA cm^{-2}), good rate capacitance (38.41% capacitance retention at 40 mA cm^{-2}) and excellent cycling stability (92.1% capacitance retention 6000 cycles at 10 mA cm^{-2}). As a result, such high performance $NiCo_2S_4$/KB nanocomposite electrode is a promising electrode for practical applications. Moreover, it may promotes a facile interface design method for controlling the mass loading of electrodes, which are useful for the fabrication of high-performance energy storage devices.

Acknowledgements

This work was supported by National Natural Science Foundation of China (21353003), Special Innovation Talents of Harbin Science and Technology (2013RFQXJ145), Fundamental Research Funds of the Central University (HEUCFZ), Key Program of the Natural Science Foundation of Heilongjiang Province (ZD201219), Program of International S&T Cooperation special project (2013DFA50480).

References

1. P. Simon, Y. Gogotsi and B. Dunn, *Science*, 2014, **343**, 1210-1211.
2. J. R. Miller and P. Simon, *Science*, 2008, **321**, 651-652.
3. P. Simon and Y. Gogotsi, *Nat. Mater.*, 2008, **7**, 845-854.
4. K. Chen, C. Sun and D. Xue, *Phys. Chem. Chem. Phys.*, 2015, **17**, 732-750.
5. M. Jin, G. Zhang, F. Yu, W. Li, W. Lu and H. Huang, *Phys. Chem. Chem. Phys.*, 2013, **15**, 1601-1605.
6. B. Mu, W. Zhang, S. Shao and A. Wang, *Phys. Chem. Chem. Phys.*, 2014, **16**, 7872-7880.
7. T. Peng, Z. Qian, J. Wang, L. Qu and P. Wang, *Phys. Chem. Chem. Phys.*, 2015, **17**, 5606-5612.
8. A. J. Roberts, A. F. Danil de Namor and R. C. Slade, *Phys. Chem. Chem. Phys.*, 2013, **15**, 3518-3526.
9. Z. Wang, Z. Li, J. Feng, S. Yan, W. Luo, J. Liu, T. Yu and Z. Zou, *Phys. Chem. Chem. Phys.*, 2014, **16**, 8521-8528.
10. C. Yang, M. Zhou and Q. Xu, *Phys. Chem. Chem. Phys.*, 2013, **15**, 19730-19740.
11. L. Yu, N. Shi, Q. Liu, J. Wang, B. Yang, B. Wang, H. Yan, Y. Sun and X. Jing, *Phys. Chem. Chem. Phys.*, 2014, **16**, 17936-17942.
12. F. Zhang, D. Zhu, X. Chen, X. Xu, Z. Yang, C. Zou, K. Yang and S. Huang, *Phys. Chem. Chem. Phys.*, 2014, **16**, 4186-4192.
13. H. Chen, J. Jiang, L. Zhang, H. Wan, T. Qi and D. Xia, *Nanoscale*, 2013, **5**, 8879-8883.
14. H. Z. Wan, J. J. Jiang, J. W. Yu, K. Xu, L. Miao, L. Zhang, H. C. Chen and Y. J. Ruan, *Crystengcomm*, 2013, **15**, 7649-7651.
15. J. Xiao, L. Wan, S. Yang, F. Xiao and S. Wang, *Nano Lett.*, 2014, **14**, 831-838.
16. H. C. Chen, J. J. Jiang, L. Zhang, D. D. Xia, Y. D. Zhao, D. Q. Guo, T. Qi and H. Z. Wan, *J. Power Sources*, 2014, **254**, 249-257.
17. W. Chen, C. Xia and H. N. Alshareef, *ACS nano*, 2014, **8**, 9531-9541.
18. J. Pu, T. T. Wang, H. Y. Wang, Y. Tong, C. C. Lu, W. Kong and Z. H. Wang, *ChemplusChem*, 2014, **79**, 577-583.
19. L. F. Shen, J. Wang, G. Y. Xu, H. S. Li, H. Dou and X. G. Zhang, *Adv Energy Mater.*, 2015, **5**.
20. Y. Zhang, C. Sun, H. Su, W. Huang and X. Dong, *Nanoscale*, 2015, **7**, 3155-3163.
21. Y. R. Zhu, Z. B. Wu, M. J. Jing, X. M. Yang, W. X. Song and X. B. Ji, *J. Power Sources*, 2015, **273**, 584-590.
22. V. H. Nguyen, C. Lamiel and J. J. Shim, *Electrochim. Acta*, 2015, **161**, 351-357.
23. Y. L. Xiao, Y. Lei, B. Z. Zheng, L. Gu, Y. Y. Wang and D. Xiao, *Rsc Adv.*, 2015, **5**, 21604-21613.
24. J. Yang, M. Z. Ma, C. C. Sun, Y. F. Zhang, W. Huang and X. C. Dong, *J. Mater. Chem. A*, 2015, **3**, 1258-1264.
25. T. Peng, Z. Y. Qian, J. Wang, D. L. Song, J. Y. Liu, Q. Liu and P. Wang, *J. Mater. Chem. A*, 2014, **2**, 19376-19382.
26. L. Yu, C. X. Zhao, X. Long and W. Chen, *Micropor. Mesopor. Mat.*, 2009, **126**, 58-64.
27. G. Zhang and X. W. Lou, *Adv. Mater.*, 2013, **25**, 976-979.
28. Z. Y. Qian, T. Peng, L. T. Qu, J. Wang and P. Wang, *J. Mater. Chem. A*, 2014, **2**, 4894-4898.
29. P. Agbo, J. R. Heath and H. B. Gray, *J. Phys. Chem. B*, 2013, **117**, 527-534.
30. S. L. Chen, H. B. Wu, H. C. Hu, Y. H. Mo, J. L. Yin, G. L. Wang, D. X. Cao, Y. M. Zhang, B. F. Yang and P. L. She, *Solid State Ionics*, 2013, **233**, 1-6.
31. T. Peng, J. Wang, Q. Liu, J. Y. Liu and P. Wang, *Crystengcomm*, 2015, **17**, 1673-1679.
32. X. Lang, A. Hirata, T. Fujita and M. Chen, *Nat. Nanotechnol.*, 2011, **6**, 232-236.
33. Y. Gogotsi and P. Simon, *Science*, 2011, **334**, 917-918.
34. J. Liu, J. Jiang, C. Cheng, H. Li, J. Zhang, H. Gong and H. J. Fan, *Adv. Mater.*, 2011, **23**, 2076-2081.
35. M. Liu, W. W. Tjiu, J. Pan, C. Zhang, W. Gao and T. Liu, *Nanoscale*, 2014, **6**, 4233-4242.

36. J. Pu, F. L. Cui, S. B. Chu, T. L. Wang, E. H. Sheng and Z. H. Wang, *Acs Sustain Chem. Eng.*, 2014, **2**, 809-815.
37. X. H. Xia, J. P. Tu, Y. Q. Zhang, Y. J. Mai, X. L. Wang, C. D. Gu and X. B. Zhao, *Rsc Adv.*, 2012, **2**, 1835-1841.
38. Y. Li, L. Cao, L. Qiao, M. Zhou, Y. Yang, P. Xiao and Y. Zhang, *J. Mater. Chem. A*, 2014, **2**, 6540.

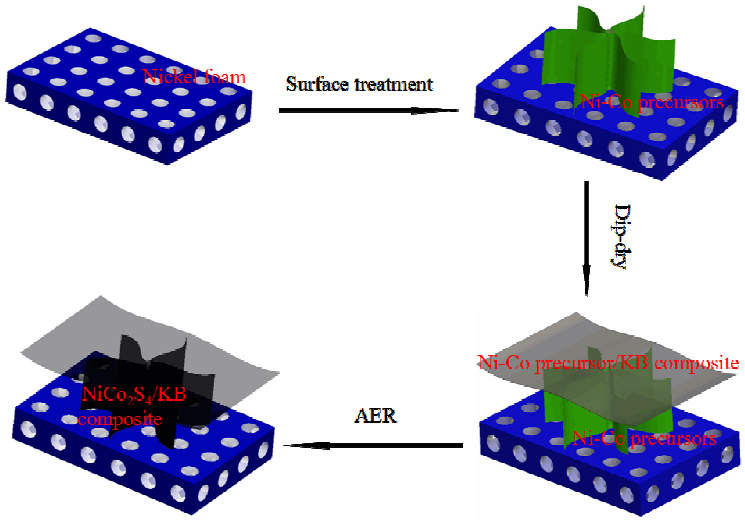

$NiCo_2S_4$/Ketjen Black nanocomposites have been successfully fabricated on nikcel foam by a facile two-step solution-based method. Electrochemical measurements demonstrate that the $Ni_1K_{0.25}$ electrode has a competitive areal specific capacitance, good rate capacitance and excellent cycling stability.